Chapter 4

VORTEX ASYMMETRIES, VORTEX WAVES

Observations of tropical cyclones indicate that storms that may be closely approximated as axisymmetric are rare - such storms tend to be the most intense and then it is usually only the inner core region that is approximately axisymmetric. The outer region of storms is invariably asymmetric, and weaker storms are usually highly asymmetric. In the previous chapter we saw how vortex asymmetries, whether they are considered a part of the vortex or a part of its environment, can influence the vortex motion.

In the following section we study the motion of initially asymmetric vortices on an f-plane. The issues to be addressed are relevant to the problem of initializing tropical cyclone forecast models as well as to an understanding of possible track changes as cyclones develop new asymmetries or as existing asymmetries evolve.

Asymmetries have implications not only for tropical cyclone motion, but also for intensification. The processes involved are intimately tied up with wave motions. Therefore in later sections we examine the dynamics of waves on vortices.

4.1 Axisymmetrization

We construct an asymmetric vortex by adding a vortex dipole to the initial vorticity distribution shown in Fig. 3.11. The vortex dipole has the form

$$\zeta_d(r,\lambda) = \zeta_D(r/d)^2 exp(-r^2/d^2) cos(\lambda - \alpha), \tag{4.1}$$

where ζ_D, d and α are prescribed constants characterizing the dipole strength, scale and orientation. Thus the vorticity maximum and minimum of the dipole occur at (d,α) and $(d,\pi+\alpha)$, respectively.

We consider four calculations with $\alpha = 0$ so that the dipole is oriented west-east. In the first calculation, S1, $d = \sqrt{2}$ and $\zeta_D = 0.2\zeta_o$, the latter being the maximum value of zeta in the symmetric vortex. In the second calculation, S2, $d = 2\sqrt{2}$ and $\zeta_D = 0.1\zeta_o$ so that the velocity at the origin associated with the dipole is the same as

in S1[1]. These two calculations are carried out on an f-plane. The third and fourth calculations, S3 and S4, are the same as S1 and S2, but are for a β-plane. The calculations are carried out numerically by a direct integration of Eq. 3.1 with the initial vorticity distribution (symmetric vortex plus dipole) described above. The Kasahara-Platzman partitioning scheme is used to analyzing the subsequent vortex evolution so that the asymmetric component of the vortex is regarded as a part of the environment, even at the initial instant. Figure 4.1 shows the evolution of the asymmetric vorticity component and associated streamfunction at selected times for the calculations S1. It can be seen that within a circle of radius about $2r_{max}$ centred on the vortex, the asymmetric vorticity field undergoes rapid distortion due to the relatively large shear of the tangential wind field in this region. For example, for the flow parameters chosen, the angular velocity of the symmetric vortex decreases monotonically with radius (see Fig. 3.3b) so that in 6 h an air parcel of 20 km radius completes approximately 2-4 revolutions compared with 1-4 revolutions at 100 km (i.e. r_{max}) and 0-5 revolutions at 200 km. Outside this circle, the distortion of the asymmetry proceeds more slowly. Initially, the asymmetric flow across the vortex is towards the south Fig. 4.1a, but its direction rotates counterclockwise with the gyres of the asymmetric streamfunction as the vorticity asymmetry is rotated. Therefore the vortex track forms a counterclockwise arc as shown in Fig. 4.2a.

As the asymmetric vorticity distribution is wound around the vortex by the angular shear of the tangential wind, the associated flow is reduced in strength and after about 12 h, the vortex essentially stalls. The reduction in strength of the asymmetric flow as the asymmetric vorticity field suffers angular shear can be understood in terms of an analytic solution for the problem in which the motion of the basic vortex is ignored. Then, in the same spirit as the calculation leading to (3.13), we can show that the asymmetric vorticity distribution at time t is given by

$$\zeta_a(r,\lambda,t) = \zeta_D(r/d)^2 exp(-r^2/d^2) cos(\lambda - \Omega(r)t). \tag{4.2}$$

For an unbounded domain, we can solve the Poisson equation for the associated streamfunction using 3.15. Using complex notation the velocity of the asymmetric flow across the vortex centre, $U_o + iV_o$, may be shown to have the form

$$U_o + iV_o = -i\zeta_D r_{\max} \int_0^\infty (\eta s)^2 \exp[-\eta^2 s^2 + i(V_{\max} t/r_{\max})\Omega'(s)] ds, \tag{4.3}$$

where $\eta = r_{max}/d$ and $\Omega'(s) = r_{\max}\Omega(r)/V_{\max}$. For large values of t (i.e. $t \geq r_{\max}/V_{\max} = 42$ min), the integrand in (4.3) oscillates rapidly. As t increases, these oscillations become more numerous and as a result of cancellation the integral itself decreases monotonically in value.

Figure 4.3 shows the evolution of the asymmetric vorticity field for calculation S2 and Fig 4.2b shows the vortex track in this simulation. As expected, since the asymmetry is concentrated at a larger radius than S1, it is less rapidly wound up

[1]See Smith *et al.* (1990), Appendix B, Eq. (B8)

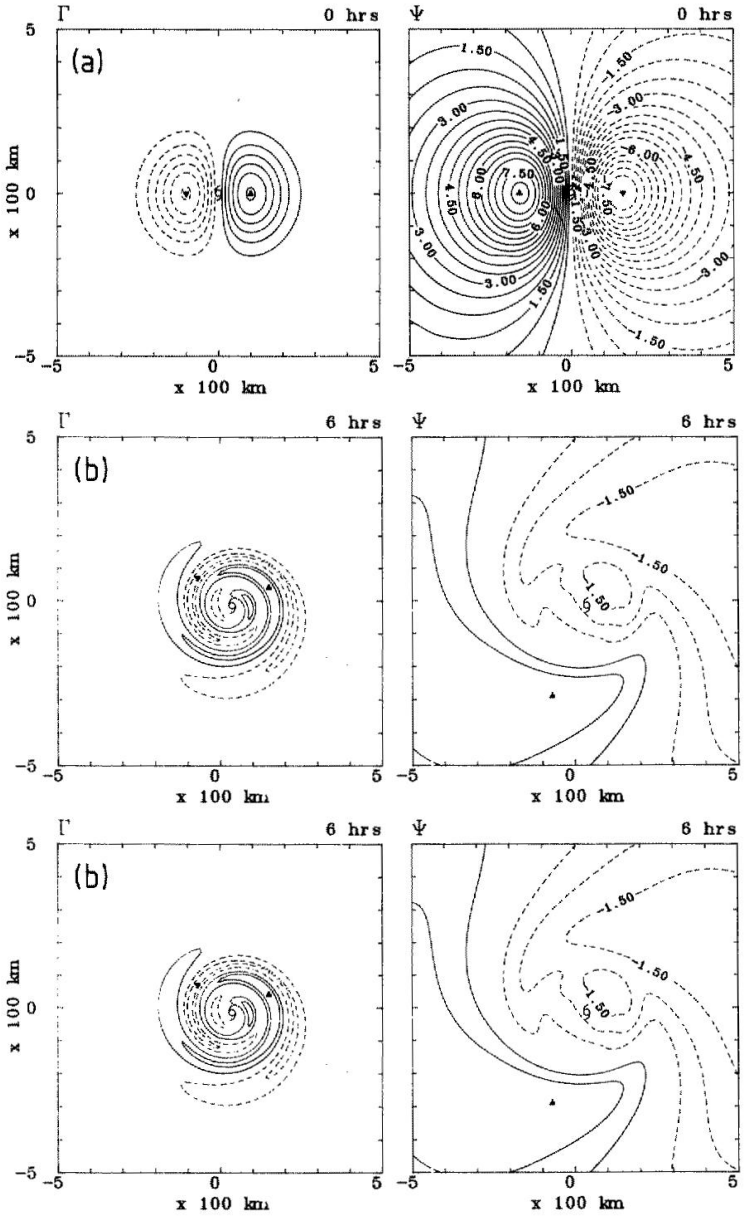

Figure 4.1: Evolution of the asymmetric vorticity field (ζ_a) and corresponding streamfunction field for the initially asymmetric vortex on an f-plane in the case of small-scale asymmetry (calculation S1), Shown are (a) the initial fields, and the fields at (b) 6 h and (c) 12 h. Note that only one quarter of the total flow domain is shown. Contour intervals are 2×10^{-5} s^{-1} for ζ_a and 5×10^4 m^2 s^{-1} for ψ_a. Zero contours have been excluded.

by the radial shear of the basic vortex. Accordingly, the asymmetric component of flow across the streamfunction centre rotates less rapidly and decays less rapidly in strength. As a result, the vortex moves farther from its initial position than in S1

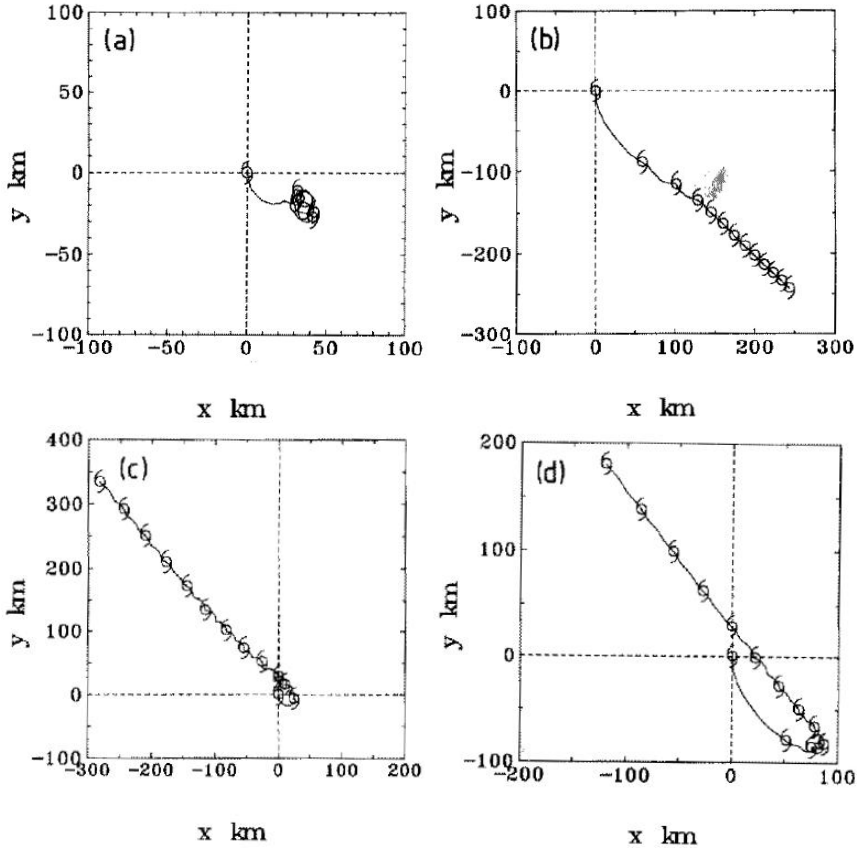

Figure 4.2: Tracks of initially asymmetric vortices in the calculations Sl to S4 defined in the text. (a) Small asymmetry, f-plane; (b) large asymmetry, f-plane; (c) small asymmetry, β-plane; and (d) large asymmetry, β-plane.

and its track rotates only slowly towards the east after the first three hours, As might be anticipated from the results of section 3.3.2. the effect of a nonzero beta would be to induce an east-west vorticity tendency in addition to the existing asymmetry. This is confirmed by the calculations S3 and S4, the vortex tracks for which are shown in panels (c) and (d) of Fig. 4.2. In S3 the vortex no longer stalls after 12 h, but recurves to move along a north-westwards track as the beta-induced asymmetries begin to dominate. In S4, the beta effect becomes important also, but not so rapidly, and again the track turns north-westwards as it does so. These calculations show that the importance of vortex asymmetry on the track depends strongly on the scale of the asymmetry. The larger this scale, the less rapidly can the asymmetry be wound up by the vortex circulation and the more persistent is the effect of the asymmetry. It is evident that initial asymmetries concentrated outside the radius of maximum tangential wind can have a significant effect on subsequent vortex positions and would need to be resolved or somehow represented in tropical-cyclone forecast models.

The asymmetries we investigated analytically in Chapter 3 were associated wholly

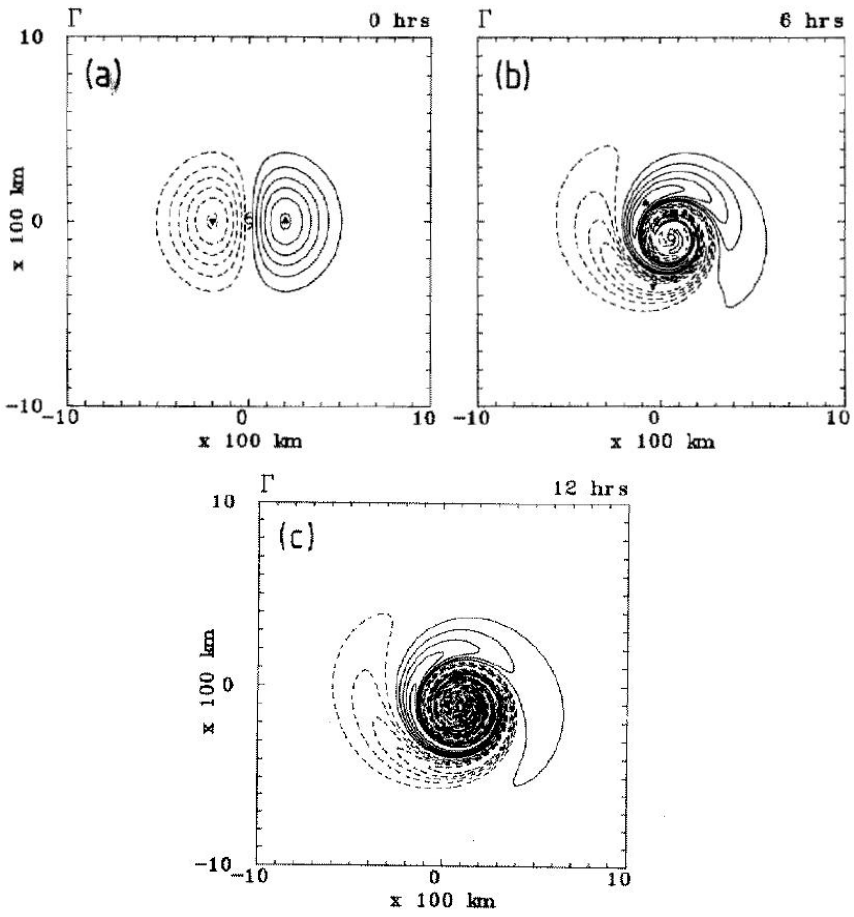

Figure 4.3: Evolution of the asymmetric vorticity field (Γ) for the initially asymmetric vortex on an f-plane in the case of large-scale asymmetry (simulation S2). Shown are (a) the initial field, and the fields at (b) 6 h and (c) 12 h. Contour interval is 1×10^{-5} s^{-1}. Note: the domain size is twice that shown in Fig. 11. Zero contours have been excluded.

with advective processes since we made the assumption that to a first approximation, the vorticity perturbation is advected by the tangential velocity of the initial axisymmetric vortex. This assumption precludes the existence of waves that propagate on the vorticity gradient of the basic vortex. However, in some situations, wave motions may be important to the dynamics and in this section we review the pertinent aspects of waves on vortices. We begin with two-dimensional non-divergent inviscid flow on an f-plane as the prototype model and go on in later sections to examine waves in a shallow-water model.

4.2 Vortex Rossby waves

We consider here the linear theory of waves on a circular vortex in gradient balance. In a stationary cylindrical coordinate-system, the linearized vorticity-equation is

$$\left(\frac{\partial}{\partial t}+\frac{\bar{v}}{r}\frac{\partial}{\partial \lambda}\right)\zeta' - \frac{1}{r}\frac{\partial \psi'}{\partial \lambda}\frac{d\bar{\eta}}{dr} = 0, \tag{4.4}$$

where ψ' denotes the perturbation streamfunction, $\zeta' = \nabla^2\psi'$ is the perturbation vorticity, $V(r)$ the basic-state tangential velocity at radius r, and $\bar{\eta} = f + (1/r)(d(rV)/dr)$ the basic-state absolute vorticity. If f is a constant, it does not appear in the problem. When (4.4) has been solved for ψ', the perturbation radial and azimuthal winds are obtained from

$$u' = -\frac{1}{r}\frac{\partial \psi'}{\partial \lambda}, \quad v' = \frac{\partial \psi'}{\partial r}. \tag{4.5}$$

The solution to (4.4) may be obtained by an azimuthal Fourier analysis. Let

$$\psi' = \hat{\psi}_n(r,t)e^{in\lambda},$$

where $\hat{\psi}_n(r,t)$ denotes the Fourier amplitude of the azimuthal wave-number n, and let $\bar{\Omega} = \bar{v}/r$ be the local angular rotation rate of the basic-state vortex. Then the linearized vorticity equation in Fourier space becomes

$$\left(\frac{\partial}{\partial t}+in\bar{\Omega}\right)\left[\frac{1}{r}\frac{\partial}{\partial r}\left(r\frac{\partial \hat{\psi}_n}{\partial r}\right)-\frac{n^2}{r^2}\hat{\psi}_n\right] - \frac{in}{r}\hat{\psi}_n\frac{d\bar{\eta}}{dr} = 0. \tag{4.6}$$

Under certain circumstances n turns out to be complex, in which case there exist unstable solutions. It can be shown that a necessary condition for the existence of unstable solutions is that the radial gradient of the basic state vorticity, $d\bar{\eta}/dr$ changes sign somewhere within the flow. We defer consideration of the unstable case until section 4.4.

A formal solution to the general initial value problem for Eq. (4.6) may be obtained using Laplace transform techniques. The Laplace transform of an arbitrary function $\chi(r,t)$ is defined by

$$\hat{\chi}(r,s) = \int_0^\infty e^{-st}\chi(r,t)dt, \tag{4.7}$$

and if $\hat{\chi}(r,s)$ is known, the inverse transform is obtained as a contour integral in the complex plane:

$$\chi(t) = \frac{1}{2\pi i}\int_{c-i\infty}^{c+i\infty} e^{st}\hat{\chi}(s)dt, \tag{4.8}$$

where c is a constant so that the contour of integration in the complex s-plane lies to the right of all singularities of $\hat{\chi}(s)$. It is easy to show that the Laplace transform

of $\partial\chi/\partial t$ is $s\hat{\chi}(r,s) - \chi(r,0)$ and it follows that the Laplace transform of Eq. (4.6) satisfies the ordinary differential equation

$$(s + in\Omega(r)) \left[\frac{1}{r}\frac{\partial}{\partial r}\left(r\frac{\partial}{\partial r}\right) - \frac{n^2}{r^2}\right]\hat{\psi}(r,s) - in\frac{d\bar{\eta}}{dr}\hat{\psi}(r,s) = \left[\frac{1}{r}\frac{\partial}{\partial r}\left(r\frac{\partial}{\partial r}\right) - \frac{n^2}{r^2}\right]\psi(r,0) \tag{4.9}$$

Dividing by $s + in\Omega(r)$ and noting that the right-hand-side of (4.9) is the initial vorticity $\hat{\zeta}_o$ of the n-th Fourier component, we obtain

$$\left[\frac{1}{r}\frac{\partial}{\partial r}\left(r\frac{\partial}{\partial r}\right) - \frac{n^2}{r^2}\right]\hat{\psi}(r,s) - in\frac{d\bar{\eta}}{dr}\frac{\hat{\psi}(r,s)}{(s + in\Omega(r))} = \frac{\zeta(r,0)}{(s + in\Omega(r))} \tag{4.10}$$

In principle, when this equation has been solved for $\hat{\psi}(r,s)$, the inverse transform must be obtained for $\psi(r,t)$. This inverse transform involves the evaluation of contour integrals in the complex plane. Using the calculus of residues we know that that the general solution consists of:

- a sum of discrete exponentials (or normal modes) associated with the zeros of the Wronskian,
- an integral along branch cuts associated with the zeros of $(s + in\Omega(r))$ that characterizes the continuous spectrum.

Explicit solutions have been obtained only in a few special cases, but an examination of these cases is instructive.

Case I: Bounded Rankine vortex: $\bar{v} = \Gamma/r, \quad \bar{\Omega} = \Gamma/r^2, \quad \Gamma = \text{constant}, \; a \le r \le b.$ In this case $d\bar{\eta}/dr = 0$ and Eq. (4.6) becomes

$$\left(\frac{\partial}{\partial t} + \frac{in\Gamma}{r^2}\right)\left[\frac{1}{r}\frac{\partial}{\partial r}\left(r\frac{\partial\hat{\psi}_n}{\partial r}\right) - \frac{n^2}{r^2}\hat{\psi}_n\right] = 0. \tag{4.11}$$

The inverse Laplace transform of (4.11) is

$$\left[\frac{\partial}{\partial r}\left(r\frac{\partial}{\partial r}\right) - \frac{n^2}{r}\right]\psi(r,t) = r\zeta(r,0)e^{-iant/r^2}. \tag{4.12}$$

The solution of this equation in the domain $a \le r \le b$ is

$$\psi(r,t) = \int_a^b G(r,x)\zeta(r,0)e^{-iant/x^2}x\,dx, \tag{4.13}$$

where the Green's function is given by

$$G(r,x) = \frac{1}{2nr^n(a^{2n} - b^{2n})}\begin{cases} (x^n - b^{2n}x^{-n})(a^{2n} - r^{2n}), & a \le r \le x \\ (x^n - a^{2n}x^{-n})(b^{2n} - r^{2n}), & x \le r \le b \end{cases} \tag{4.14}$$

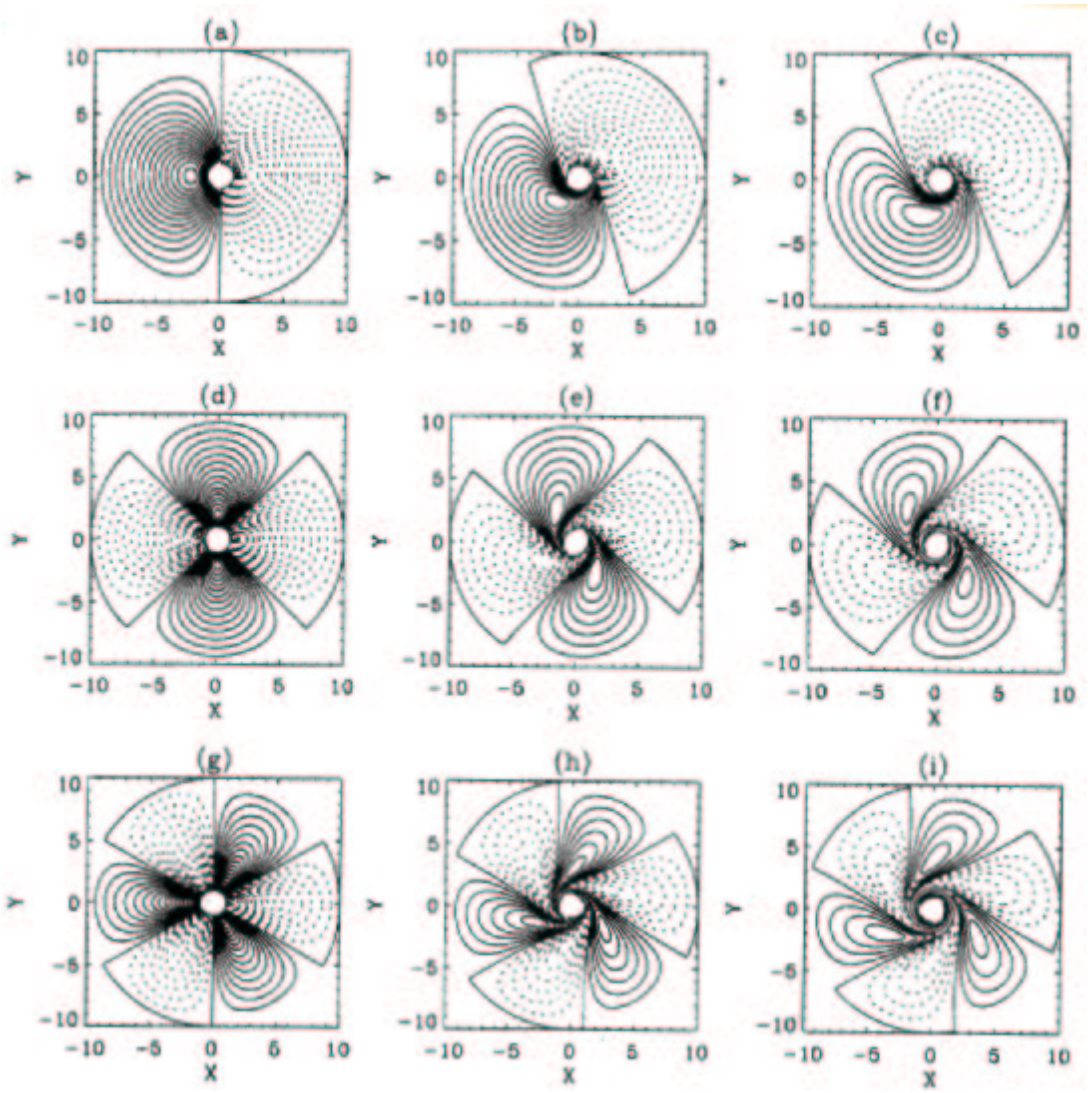

Figure 4.4: Perturbation streamfunction field for $\zeta(r,0) = 1/r^3$ for the hounded Rankine vortex in the region $a = 1, b = 10$. The columns show contours at times $t = 0$, $t = 3.6$ and $t = 7.2$, respectively. Panels (a)-(c) show contours for $n = 1$ where the contour interval is 1.1×10^{-2}. Panels (d)-(f) show contours for $n = 2$ where the contour interval it 5.67×10^{-3}. Panels (g) - (i) show contours for $n = 3$ where the contour interval is 3.31×10^{-3}.

Finally, the Fourier inversion for wavenumber n is

$$\psi_n(r,\lambda,t) = e^{in\lambda} \int_a^b G(r,x)\zeta(r,0)e^{-iant/x^2} x dx. \tag{4.15}$$

Some solutions for various initial distributions of $\zeta(r,0)$ and n are given by Smith and Montgomery (1995). Figure 4.4 shows shows the streamfunction fields for an

upright distribution of initial vorticity $\zeta(r,0) = 1/r^3$ and Fig. 4.5 shows the corresponding vorticity fields. The rows represent wavenumbers $n = 1, 2$ and 3 respectively, while the columns designate times $t = 0$, $t = 3.6$ and $t = 7.2$, respectively. These figures show how the initial disturbances are sheared out preferentially in the inner region of the vortex by the large angular shear of the vortex. However, unlike in the calculations in Chapter 3, wave dynamics are involved on account of the term $u(d\bar{\eta}/dr)$ that is retained at first-order in Eq. (4.4). The solutions are cylindrical analogues of plane wave solutions describing sheared disturbances in rectangular simple shear flow (see e.g. Smith and Montgomery, 1995). Physically pertinent properties of these solutions, such as the dependence of integrated kinetic energy on azimuthal wave-number, are examined by Smith and Montgomery *op. cit.*.

Case II: Unbounded Rankine vortex: $\bar{\eta}$ discontinuous at $r = r_{max}$

The Rankine vortex is defined by the profile

$$V(r) = \begin{cases} r/a, & r \leq a, \\ a/r, & a \leq r, \end{cases} \tag{4.16}$$

where a is the radius of maximum winds. The corresponding profile of basic-state vorticity is

$$\bar{\zeta}(r) = \begin{cases} 2/a, & r < a, \\ 0, & a < r, \end{cases} \tag{4.17}$$

The profile of absolute vorticity is

$$\bar{\zeta}(r) = \begin{cases} Ro^{-1} + 2/a, & r < a, \\ Ro^{-1}, & a < r, \end{cases} \tag{4.18}$$

where Ro is the Rossby number $= V_m/R_m$. The discontinuity in the mean-state vorticity at $r = a$ effectively introduces another boundary to the system. Since this boundary lies in the interior of the fluid, kinematic and dynamic boundary conditions must be satisfied at the disturbed interface $r = a + \xi$, where ξ is the interface displacement. The kinematic boundary condition requires that the normal velocity be continuous at $r = a + \xi$ while the dynamic boundary condition requires that the pressure be continuous at this radius. Consistent with the linearization of the equations, the matching conditions can be evaluated at $r = a$. Once u is determined, the evolution of the disturbed interface may be found by integrating

$$\left(\frac{\partial}{\partial t} + \frac{\overline{v}}{r}\frac{\partial}{\partial \lambda}\right)\xi = u \tag{4.19}$$

for ξ at $r = a$.

For the full Rankine profile (4.17) the linearized vorticity equation (4.4) is modified to

$$\left(\frac{\partial}{\partial t} + \frac{\overline{v}}{r}\frac{\partial}{\partial \lambda}\right)\zeta = 0 \quad r \neq a. \tag{4.20}$$

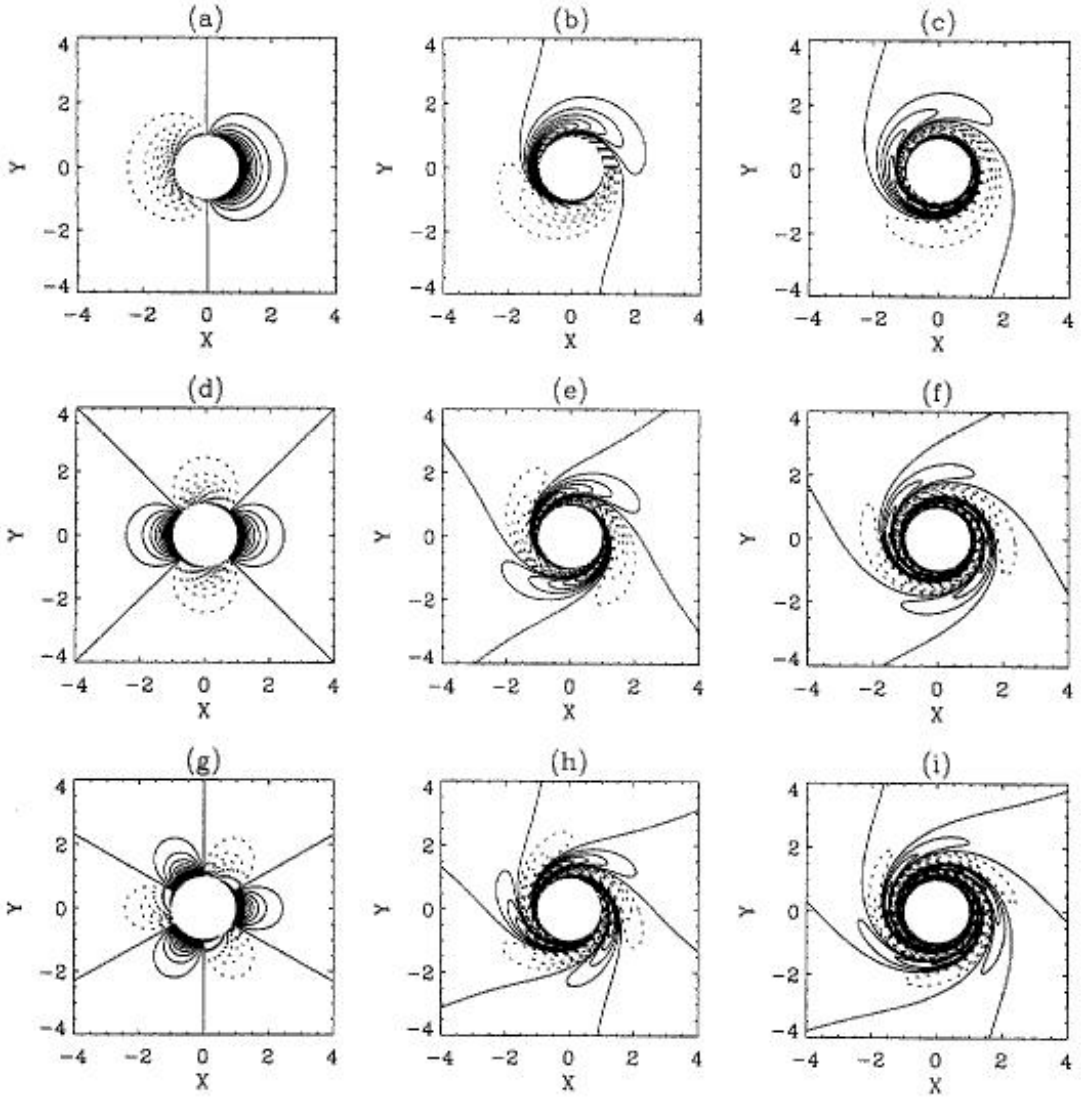

Figure 4.5: Perturbation vorticity-field corresponding to Fig. 9. The contour interval is 6.9×10^{-2}.

To solve (4.20), the discontinuity in the basic-state vorticity at $r = a$ must be accounted for. Since the problem is linear, the superposition principle may be used to separate the solution into two parts by letting $\zeta = \zeta_s + \zeta_1$, where ζ_s. is defined to be smooth for all r and ζ_i accounts for the discontinuity in the basic-state vorticity at $r = a$. The vorticity equation (4.20) is then split into two parts

$$\left(\frac{\partial}{\partial t} + \frac{\overline{v}}{r}\frac{\partial}{\partial \lambda}\right)\zeta_s = 0 \quad \forall\, r \tag{4.21}$$

$$\left(\frac{\partial}{\partial t} + \frac{\overline{v}}{r}\frac{\partial}{\partial \lambda}\right)\zeta_1 = 0 \quad r \neq a. \tag{4.22}$$

Equation (4.21) is formally identical to the system solved in Case I, but with the foregoing boundary conditions. The corresponding solution in Fourier space is

$$\hat{\psi}_s(r,t) = \int_0^\infty G(r,\rho)\hat{\zeta}_{s0}(\rho)e^{-in\bar{v}/\rho}\rho d\rho \tag{4.23}$$

where the appropriate Green's function is

$$G(r,t) = -\frac{1}{2n}\begin{cases} \rho^{-n}r^n, & 0 \le r \le \rho \\ \rho^n r^{-n}, & \rho \le r \le \infty \end{cases} \tag{4.24}$$

and $\hat{\zeta}_{s0}(\rho)$ is the smooth component of $\hat{\zeta}$ throughout the vortex at time $t = 0$.

The Fourier-space equivalent to (4.22) is

$$\left(\frac{\partial}{\partial t} + \frac{in\bar{v}}{r}\right)\hat{\zeta}_1 = 0, \quad r \neq a. \tag{4.25}$$

Anticipating that the solution to (4.25) will yield the discrete normal modes which are irrotational on both sides of the mean-state vorticity discontinuity, $\hat{\zeta}_1$ is assumed to be separable and of the form

$$\hat{\zeta}_1 = \gamma(t)\delta(r-a). \tag{4.26}$$

Here, γ is an undetermined temporal multiplier for $\hat{\zeta}_1$, and $\delta(r-a)$ is the Dirac delta function. In terms of the perturbation streamfunction, (4.26) becomes

$$\nabla^2\hat{\psi}_1 = \gamma(t)\delta(r-a). \tag{4.27}$$

The streamfunction is also assumed to be separable and of the form $\hat{\psi}_1 = \gamma(t)\hat{\Psi}_1(r)$. Thus, (4.27) becomes

$$\left(\frac{1}{r}\frac{d}{dr}\left(r\frac{d}{dr}\right) - \frac{n^2}{r^2}\right)\hat{\Psi}_1 = \delta(r-a). \tag{4.28}$$

For $r \neq a$, (4.28) is Euler's equation. Two conditions are needed to match the solutions in each region across $r = a$. The first is the kinematic boundary condition requiring that the radial velocity u be continuous at $r = a$. Consequently, the Fourier streamfunction amplitude must be continuous across $r = a$. The second condition results from integrating (5.12) over a small interval that includes r = a. This yields the following jump condition for $\hat{\psi}_1$

$$\frac{d}{dr}\hat{\Psi}_1 r(a^+) - \frac{d}{dr}\hat{\Psi}_1 r(a^-) = 1. \tag{4.29}$$

Applying the boundary conditions, and the continuity and jump conditions at $r = a$, yields

$$\hat{\Psi}_1 = -\frac{a}{2n}\begin{cases} a^{-n}r^n, 0 \le r \le a \\ a^n r^{-n}, a \le r \le \infty, \end{cases} \tag{4.30}$$